Romanian Reports in Physics, Vol. 66, No. 3, P. 630–648, 2014

ATOMIC PHYSICS

K X-RAY PRODUCTION AND REC CROSS SECTIONS IN 0.75 –2.5 MeV/u ^{32}S, ^{35}Cl IONS ON Cu ATOMIC COLLISIONS

A.C. SCAFEŞ, C. CIORTEA, D.E. DUMITRIU, A. ENULESCU, D. FLUERAŞU, M.M. GUGIU, M.D. PENA, M. PENȚIA, and I. PITICU

"Horia Hulubei" National Institute for Physics and Nuclear Engineering (IFIN-HH), P.O.Box MG-6 Măgurele, 077125 Bucharest, Romania
E-mail: ascafes@tandem.nipne.ro; ccio@nipne.ro

Received August 26, 2013

Abstract. From the measured target thickness dependences of K X-ray and radiative electron capture (REC) yields for 0.75 – 2.5 MeV/u ^{32}S, ^{35}Cl + Cu collisions, the K X-ray production for both partners and REC cross sections, in dependence of collision energy, have been determined. In comparison with theory, we find several simple models which describe rather well some of the present results. The present target (Cu) K X-ray production cross sections are in fair agreement with ECPSSR model predictions, for both collision systems. The REC theoretical predictions (Stobbe calculations times 11, the number of "loosely" bound electrons in Cu) are in good agreement with the present data. The analysis of L- and M-shell multiple ionization as well as of target thickness dependence allowed estimating the outer-shell multiple ionization probabilities per electron of both collision partners as well as the enhancements of the projectile K-shell fluorescence yields and lifetimes of one vacancy state, respectively. Large enhancements of the projectile K-shell fluorescence yields, attaining values as high as 0.5 in Cl and 0.9 in S, have been obtained. Also, increased K-shell vacancy lifetimes, by factors up to 14 for S and 20 for Cl, have been estimated.

Key words: K-shell fluorescence yields and lifetimes, K X-ray, ionization and REC cross sections, outer-shell multiple ionization probabilities.

1. INTRODUCTION

When fast heavy ions were passed through a solid target it is likely to have residual excitation in the inner electronic shells due to collision times which are shorter than the de-excitation lifetimes. More than four decades ago, Betz and Grodzins [1] suggested that such excitation could largely account for the observation that the equilibrium charge state of an ion after penetrating a solid

target is larger than that after coming through a dilute gas. More recently, solid-state effects by highly-charged, energetic heavy ions have been observed (see *e.g.* ref. [2] for multiple electron capture). These target density effects influence both outer- and inner-shell configurations of the projectiles, and consequently the spectroscopic properties of both collision partners and their emitted radiations [3].

Experimentally, in some energetic atomic collisions a strong enhancement in the target K X-ray yield was observed for the $q = Z_1 - 1$ or Z_1 (the charge state of the incident ion having an atomic number Z_1) in comparison to lower charge states, both for gas and solid targets [4–11]. This enhancement is due to the K-shell electron capture into the projectile K-vacancy, in addition to direct ionization. Hence, there appears for solid targets the dependence on the target effective thickness, due to variation with the target thickness of the fraction of ions having one K-vacancy.

The target thickness effects have been reported both for target and projectile X-rays, as well as for radiative electron capture (REC) (see *e.g.* ref. [8]). In those cases, where incident charge state and target thickness effects appear, in order to determine heavy-ion induced radiation yields (X-rays, Auger electons, REC), it is essential that these effects to be taken properly into account.

In the present work we present results of a study of both target and projectile K X-ray production as a function of target thickness for 0.75–2.5 MeV/u ^{32}S and ^{35}Cl ions, incident on thin targets of Cu. K-shell REC has been also determined. Preliminary results of the present paper have been communicated to the HCI 2012 Conference in Heidelberg and will be published in the Proceedings [12]. By measuring the projectile and target K X-ray production and REC yields in dependence of target effective thickness in the range of 0.1–0.5 mg/cm^2, the K X-ray production and REC cross sections in dependence of collision energy have been determined. The analysis of L- and M-shell multiple ionization as well as of target thickness dependence allowed estimating the outer-shell multiple ionization probabilities per electron of both collision partners as well as the enhancements of the projectile K-shell fluorescence yields and lifetimes of one vacancy state. The present experimental results are compared with some simple models of ionization and REC.

2. MULTIPLE IONIZATION. K X-RAY ENERGY SHIFTS

In the experimental analysis of the multiple outer-shell ionization, which is dominantly present in collision systems like those studied here, the K X-ray yield and energy shifts method was used [13]. The presence of spectator vacancies in the

outer-shells conducts to modified K_β / K_α X-ray yield ratio as well as to their energy shifts, the larger collision energy the larger numbers of spectator vacancies. Calculations show that this K X-ray yield and energy shifts could be used for estimating the mean numbers of outer (L and M) shell spectator vacancies, or equivalently of the ionization probabilities per electron (noted p_L and p_M, respectively). Here, p_L and p_M are given by $p_L = \overline{n}_L / 8$ and $p_M \equiv p_{M1-3} = \overline{n}_{M1-3} / 8$, respectively, where $\overline{n}_L$ and $\overline{n}_M$ are the corresponding mean numbers of L- and M_{1-3}-shell vacancies.

In the present work, the analysis of the outer-shell multiple ionization implied determination of outer-shell L- and M-shell ionization probabilities per electron using the "yield and energy shifts" method as well as estimation of the projectile K-shell fluorescence yield $\omega_K^{(p)}$, using the procedure in ref. [13] (which will be referred here as Piticu's formula – after the present author' name which originally developed the procedure), or the Greenberg's formula [21], as well as of the K-vacancy lifetime $\tau_K^{(p)}$ [13].

Using some approximations, the calculation of K_β / K_α X-ray ratio in dependence of p_L and p_M has been done, and the results presented before [13, 14] will be not more repeated here. In the present paper, the calculation results of K X-ray energy shifts used for estimating the ionization probabilities per electron p_L and p_M will be presented. All calculations have been done with an atomic multi-configuration Dirac – Fock code [15].

The results of analogous calculations done for S and Cl $K_{\alpha,\beta}$ X-ray energy shifts for different numbers of vacancies in the L- and M-shells are given in Fig. 3 and the mean values per vacancy in Table 2.

2.1. TARGET ATOM (Cu)

Calculations have been done for Cu^{1+} (without the N_1 – electron) or Cu^{11+} (without $M_{4,5}$ and N_1 electrons). The target (Cu) $K_{\alpha,\beta}$ X-ray energy shifts due to multiple vacancies in L-shell and M_{1-3} – subshells, as well as for one L_3 / M_3 plus $M_{4,5}$ – subshell multiple vacancies are presented in Fig. 1.

In the case of multiple vacancies, the energy shifts per vacancy depend on the number of vacancies, as shown in the figures below, where the successive differences (Fig. 2a) and the ratio of multiple per one vacancy (Fig. 2b) energy

shifts for Cu $K_{\alpha,\beta}$ X-rays are presented. Subshell structure effects (that can be seen clearly in Fig. 2a) as well as electron shielding effects (that are higher in Cu^{11+} than Cu^{1+} , as seen in Fig. 2b), explain the difference from the strict proportionality to the number of vacancies.

By linear fitting the calculated energy shifts in dependence of vacancy number, the straight line slopes give the X-ray mean energy shifts per vacancy. The results obtained for the Cu $K_{\alpha,\beta}$ X-ray mean energy shifts per vacancy in the L-shell and M_{1-3} – subshells, for different numbers of vacancies in $M_{4,5}$ – subshells, are given in Table 1. The values for 5 $M_{4,5}$ vacancies were used in the fit procedure for determination of the outer-shell multiple ionization probabilities per electron.

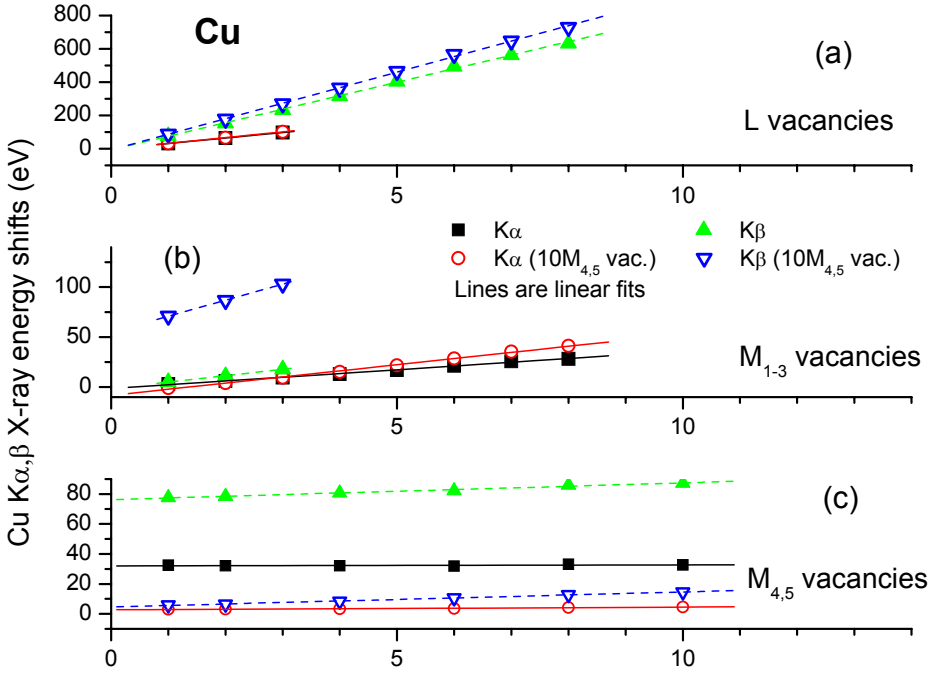

Fig. 1 – Calculated Cu $K_{\alpha,\beta}$ X-ray energy shifts due to: a) L-shell multiple vacancies; b) M_{1-3} subshell multiple vacancies; c) one L_3 / M_3 plus multiple $M_{4,5}$ – subshell vacancies. Two cases, for different numbers of L-shell vacancies in Cu^{1+} (full symbols) and in Cu^{11+} (open symbols), are presented. The symbols are explained in the figures and the lines are linear fits to the results of calculation.

Table 1

The Cu $K_{\alpha,\beta}$ X-ray mean energy shifts per vacancy in the L-shell and $M_{1\text{-}3}$-subshells, for different numbers of vacancies in $M_{4,5}$-subshells

	Mean shift per L-vacancy (eV)			Mean shift per $M_{1\text{-}3}$-vacancy (eV)		
	no $M_{4,5}$ vac.	10 $M_{4,5}$ vac.	5 $M_{4,5}$ vac.	no $M_{4,5}$ vac.	10 $M_{4,5}$ vac.	5 $M_{4,5}$ vac.
Kα	32.98	34.56	33.31	3.75	6.15	4.62
Kβ	81.14	93.19	86.73	6.42	16.04	11.42

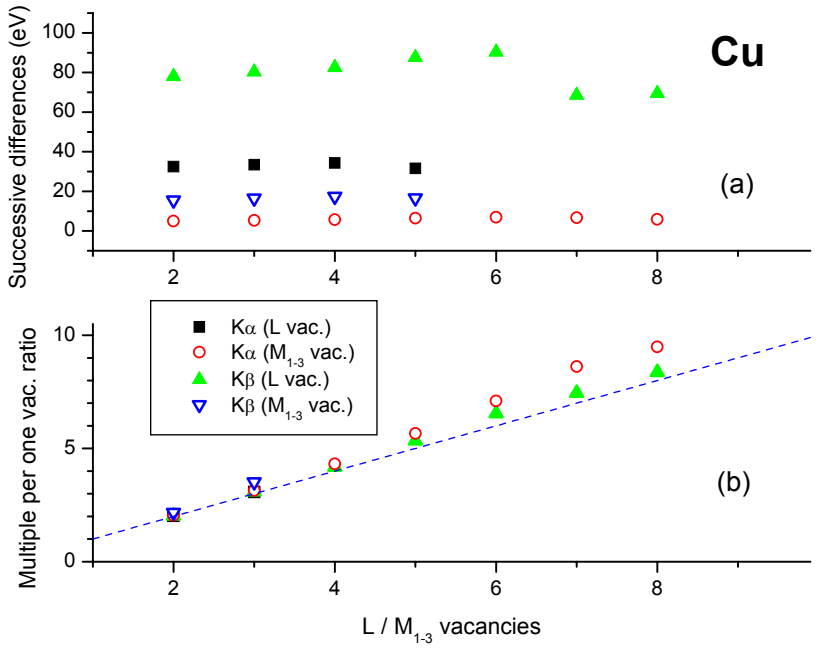

Fig. 2 – a) Successive differences of Cu $K_{\alpha,\beta}$ X-ray energy shifts for variable numbers of L-shell / $M_{1\text{-}3}$-subshell vacancies. In case of $M_{1\text{-}3}$-vacancies, empty $M_{4,5}$ -subshells were considered; b) the ratio of multiple- per one-vacancy energy shifts of $K_{\alpha,\beta}$ X-rays for variable numbers of L-shell / $M_{1\text{-}3}$-subshell vacancies. In case of $M_{1\text{-}3}$-subshells vacancies, empty $M_{4,5}$-subshells were considered. The line corresponds to the strict proportionality to the number of vacancies. The symbols are explained in the figures.

2.2. PROJECTILE IONS (S, Cl)

The results of analogous calculations done for S and Cl $K_{\alpha,\beta}$ X-ray energy shifts for different numbers of vacancies in the L- and M-shells are given in Fig. 3 and the mean values per vacancy in Table 2.

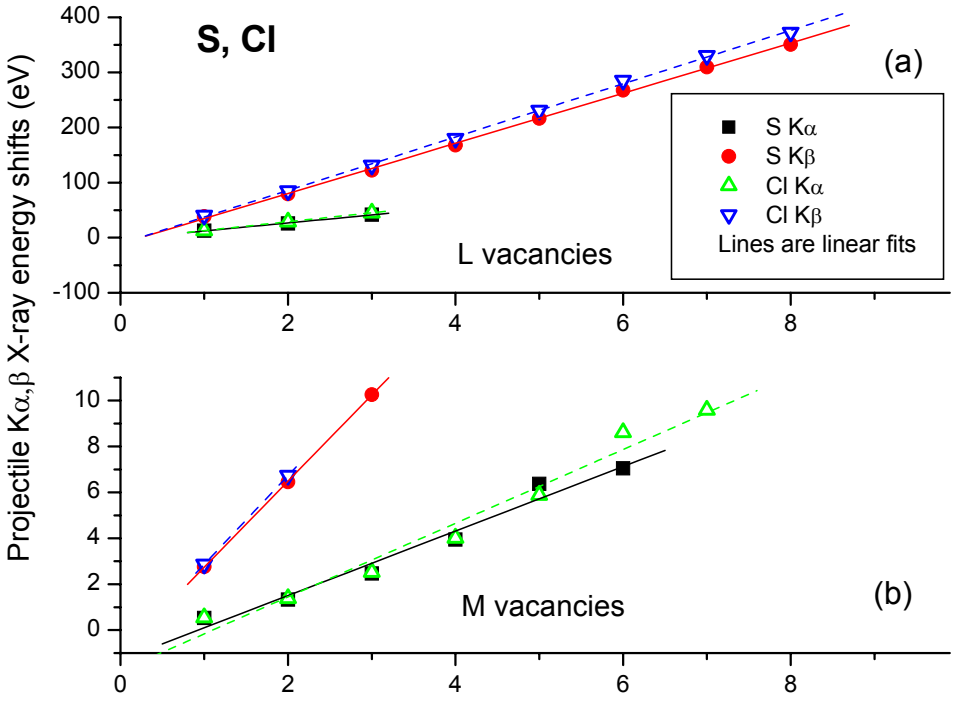

Fig. 3 – The $K_{\alpha,\beta}$ X-ray energy shifts due to multiple: a) L-shell; b) $M_{1\text{-}3}$ -subshells vacancies, for the projectile ions S (full symbols) and Cl (open symbols). The symbols are explained in the figures and the lines are linear fits to the results of calculation.

Table 2

The S and Cl $K_{\alpha,\beta}$ X-ray mean energy shifts per vacancy in the L- and M-shells

	Mean shift per L-vacancy (eV)		Mean shift per M-vacancy (eV)	
	S	Cl	S	Cl
Kα	14.53	16.20	1.405	1.605
Kβ	45.51	48.38	3.751	3.865

Subshell structure effects can be seen clearly in Fig. 4, that give the successive differences of $K_{\alpha,\beta}$ X-ray energy shifts for different numbers of L and M-shell vacancies. This explains the difference to the strict proportionality with the number of vacancies (as seen before for the target atom, Fig. 2).

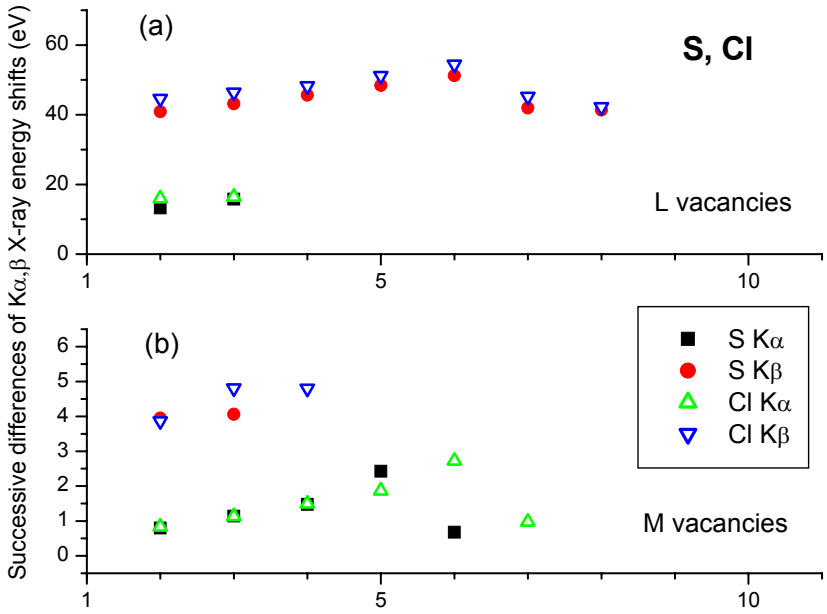

Fig. 4 – Successive differences of projectile (S and Cl) $K_{\alpha,\beta}$ X-ray energy shifts for different numbers of: a) L-shell; b) $M_{1\text{-}3}$-subshell vacancies. The symbols are explained in the figures.

3. EXPERIMENT AND DATA ANALYSIS

3.1. MEASUREMENTS

A simple apparatus and experimental method were used in the measurements conducted at the 8 MV FN-type tandem accelerator of IFIN-HH. The analyzed ions beams of $^{32}S^{q+}$ and $^{35}Cl^{q+}$ (q = 4^{+}–11^{+}) hit a self supporting Cu target of 90–100 μg/cm^2 thickness, rotated at different angles relative to the beam direction; this way, the target presents different effective thicknesses, in the range of about 100–500 μg/cm^2. The thickness of the target was determined during vacuum evaporation.

The X-rays have been measured using Si(Li) and HPGe detectors, having 180 eV and 140 eV / 5.9 keV energy resolution, respectively, placed at 90^0 to the beam direction. Except the Be windows, of the scattering chamber and detector cryostat, as well as an air gap of 6–8 cm thickness, no other X-ray absorbers have been used. The relative detector efficiencies have been calculated using photon absorption cross sections [16]. Using calibrated radioactive sources (^{241}Am), the absolute efficiencies of the X-ray detectors have been determined. Measuring

simultaneously, with both X-ray detectors allowed the estimation of the HPGe detector dead layer. Periodically, the energy calibration of the installation was verified by measuring with calibrated radioactive sources (^{55}Fe and ^{57}Co).

Using two 110 μm thick foil scintillators, placed at 90^0 and at a forward angle (about 10^0) to the beam direction, normalization of the X-ray yields to the scattered ions was done. The forward angle of the particle detector was measured by comparing the intensities obtained simultaneously with both particle detectors, and by determining their solid angles using a standard radioactive source (^{241}Am).

3.2. TARGET THICKNESS DEPENDENCE

For the strong enhancements observed in the target K X-ray yield for $q = Z_1 - 1$ in comparison to $q \le Z_1 - 2$ charge states of the incident ion [4–11], it was assumed that $\sigma_{x1}^{(t)} = \alpha\sigma_{x0}^{(t)}$, where $\sigma_{x1}^{(t)}$ and $\sigma_{x0}^{(t)}$ are the target K X-ray yields for projectiles with a K-vacancy and without a K-vacancy, respectively.

We report here K X-ray production and REC cross sections, as well as other projectile related quantities, like K-shell fluorescence yield and one vacancy lifetimes. These quantities were obtained from the measured target thickness dependences of the K X-ray and REC yields, fitted by the least-squares method to a two-component model proposed by Betz *et al.* [4].

Target and projectile X-ray yields are parameterized in function of target thickness. Because the present data could not determine uniquely all the parameters involved in eq. (2) – (5) below, we had to rely on data in the literature. For the projectiles, there were not taken into consideration that within target presumably significant fractions of few-electron metastable states could exist.

Using the notation of Tanis *et al.* [8], in the case of ions having charge states $q \le Z_1 - 2$ incident on a target of thickness T, we can write the following relations

$$F_1(x) = \frac{\sigma_v}{\sigma}(1 - \mathrm{e}^{-\sigma x}), \tag{1}$$

for the fraction of ions with one K-vacancy at a depth *x* in the target; the limit value for large target thicknesses is $F_1(\infty) = \sigma_v / \sigma$;

$$\bar{\sigma}_x^{(t)} = \sigma_{x0}^{(t)}\left\{1 + (\alpha - 1)\frac{\sigma_v}{\sigma}[1 - E(T)]\right\} \tag{2}$$

for the target K X-ray yield;

$$\bar{\sigma}_x^{(p)} = \sigma_{x0}^{(p)} E(T) + \lambda_x \frac{\sigma_v}{\sigma}[1 - E(T)] \tag{3}$$

for the projectile K X-ray yield, and

$$\bar{\sigma}_{REC} = \sigma_{R0} \frac{\sigma_v}{\sigma}[1 - E(T)] \tag{4}$$

for the K-REC yield. Here, $E(T)$ is given by $E(T) = \left(1 - e^{-\sigma T}\right)/\sigma T$, superscripts p or t refer to projectile or target, respectively, and index 0 refers to quantities corresponding to the limit of no projectile K-vacancy σ_v and $\sigma = \sigma_v + \sigma_q$ note the projectile K-vacancy production and total cross sections, respectively, where σ_q is the quenching cross section due to either electron capture into K-vacancy state of the projectile or due to decay of this state. λ_x is the projectile K-vacancy radiative decay probability per unit path length (in units of cm^2). An useful quantity, noted here $\bar{\sigma}_{REC}^{(2)}$, used for estimating λ_x from the target thickness dependence (see also *e.g.* Schulé *et al.* [17]), could be introduced by the relation:

$$\bar{\sigma}_{REC} / \bar{\sigma}_x^{(p)} = \bar{\sigma}_{REC}^{(2)} / \lambda_x ; \tag{5}$$

it depends on target thickness, and tends to σ_{R0} at large target thicknesses.

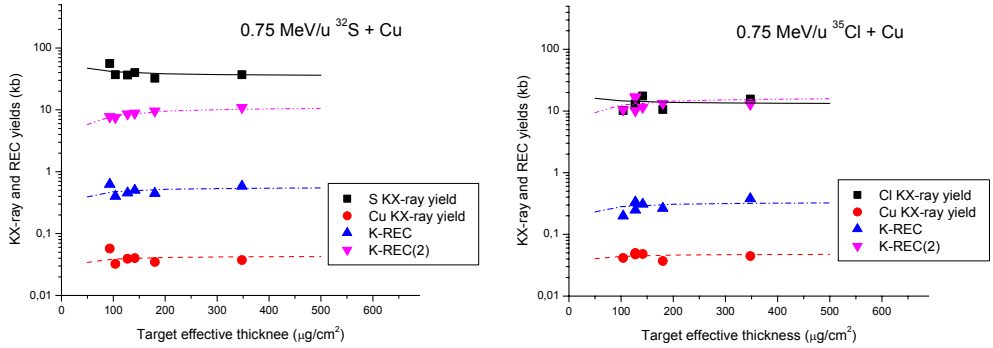

(a) (b)

Fig. 5 – K X-ray and REC yields for 0.75 MeV/u ^{32}S (a) and ^{35}Cl (b) ions bombarding thin Cu targets in dependence of target effective thickness. The symbols are explained in the figures; the lines give the fits to data by eqs. (2-5).

In Fig. 5, examples of measured target thickness dependences for K X-ray and REC yields at 0.75 MeV/u for both collision systems are presented. The lines are obtained by fitting with the eqs. (2) – (5) above.

There are more characteristic parameters involved in the target thickness dependences, which cannot be all, uniquely determined by the present target thickness dependences, measured for projectile charge states, $q < Z_1 - 2$ and at only relatively large target effective thicknesses. For some of the parameters, like the projectile K-vacancy production σ_v and total $\sigma_.$ cross sections, or the enhancement α of the target K X-ray yield, we had to rely on literature data and allow only a limited variation around them during the fitting procedure.

Only a few data in the literature for the S+ Cu collision system was found, *e.g.* Gardner *et al.* [7], where vacancy production and quenching cross sections for 1.7 MeV/u are given graphically, while more data for the Cl+ Cu collision have been reported (see *e.g.* ref. [6–8]). However, it was found that variations in the fitting parameters σ, σ_v and λ_x, *e.g.* compared to Tanis *et al.* [8] for collision Cl+ Cu, have a rather small influence on the results obtained for the K X-ray production ($\sigma_{x0}^{(p)}$, $\sigma_{x0}^{(t)}$) and REC (σ_{R0}) yields reported here. To note also that σ, σ_v/σ and $\sigma_{x0}^{(p)}$ being varied independently, the procedure of fitting in dependence on target thickness allows estimations of the projectile K-shell fluorescence yield $\omega_K^{(p)}$ independently of the outer-shell multiple ionization analysis; both procedures have been applied in the present paper.

Concerning the enhancement parameter $\alpha = \sigma_{x1}^{(t)} / \sigma_{x0}^{(t)}$, we adopted interpolated values after those reported by Tanis et al. [8] in the case of the Cl+ Cu collision. In the case of S+ Cu collision, the values of α were estimated by applying a formula found by Gray *et al.* [6] to reproduce accurately the experiment:

$$\alpha - 1 = \sigma_R \, w \omega_{Cu} / \sigma_{x0}^{t} \,, \tag{6}$$

where, $\sigma_R = \pi R^2$, with $R = 2.6/Z_2$ a.u. the radius corresponding to the peak in the dynamic coupling elements ($Q = 0.60$) given by Taulbjerg *et al.* [18] (here $Z_2 = 29$ is the atomic number of Cu), w is the Meyerhof [19] vacancy transfer probability, and $\omega_{Cu} = 0.44$ is the fluorescence yield of Cu [20]. Binding energies of the He-like projectiles are used in the calculation of w.

Regarding the errors of the reported data, we can mention the following. For generally small (≤ 5%) statistical errors, taking into account the errors in efficiency calibration (detector relative efficiency, X-ray attenuation in the windows and air, as well as the errors for radioactive source calibration), total errors of ≤ 12% could be estimated. However, the rather large dispersion of the measured dependences on target thickness, as well as the uncertainties in the fitting parameters (like σ, σ_v and λ_x) give rise to much higher fitting errors. We estimate a fitting error (one

standard deviation) of 33% for the projectile related quantities, $\sigma_{x0}^{(p)}$, $\omega_K^{(p)}$ and the K-vacancy lifetime ($\tau_K^{(p)}$), and 17% for the target $\sigma_{x0}^{(t)}$ and REC σ_{R0} cross sections reported here.

4. RESULTS AND DISCUSSION

4.1. OUTER-SHELL MULTIPLE IONIZATION ANALYSIS

In Figs. 6 and 7, the measured target (Cu) and projectile (S and Cl) $K_{\alpha,\beta}$ X-ray energy shifts and K_β / K_α X-ray yields ratios in the collisions ^{32}S, ^{35}Cl + Cu in dependence of collision energy are given.

By applying the yield and energy shifts method, the obtained L- and M-shell multiple ionization probabilities per electron (p_L and p_M, respectively) are given in Fig. 8, and compared with the geometric model (GM) [22] predictions in the Figs. 9 for Cu and 10 for S and Cl. Corrected GM (corr. GM) stands for calculations with increased binding energies, corresponding to the final spectator vacancy configurations.

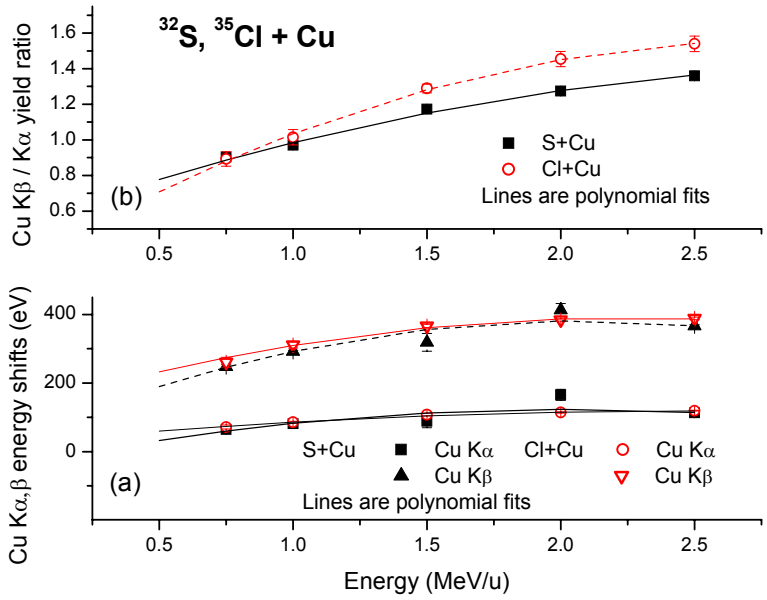

Fig. 6 – Cu $K_{\alpha,\beta}$ X-ray energy shifts (a) and K_β / K_α X-ray yields ratios (b) in the collisions ^{32}S + Cu (full symbols) and ^{35}Cl + Cu (open symbols), in dependence of collision energy. The lines are fits to experimental data.

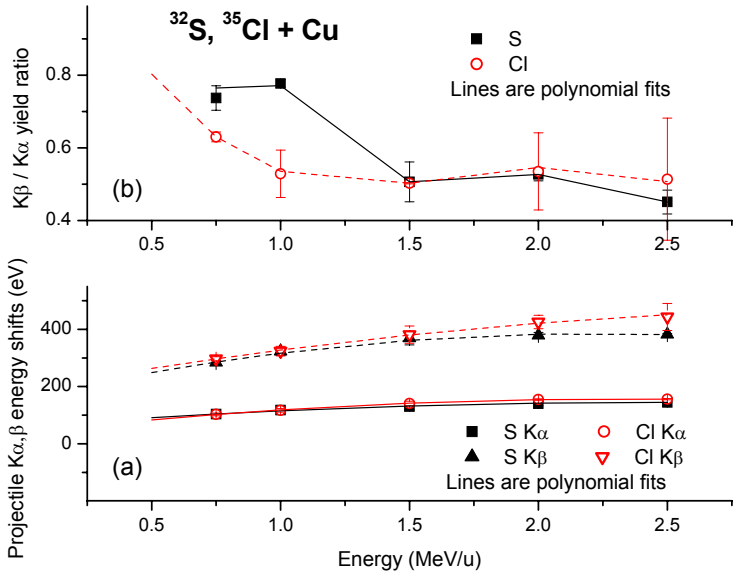

Fig. 7 – Projectile (S and Cl, full and open symbols, respectively) $K_{\alpha,\beta}$ X-ray energy shifts (a) and K_{β}/K_{α} X-ray yields ratios (b) in the ^{32}S, ^{35}Cl + Cu collisions, in dependence of collision energy. The lines are fits to experimental data.

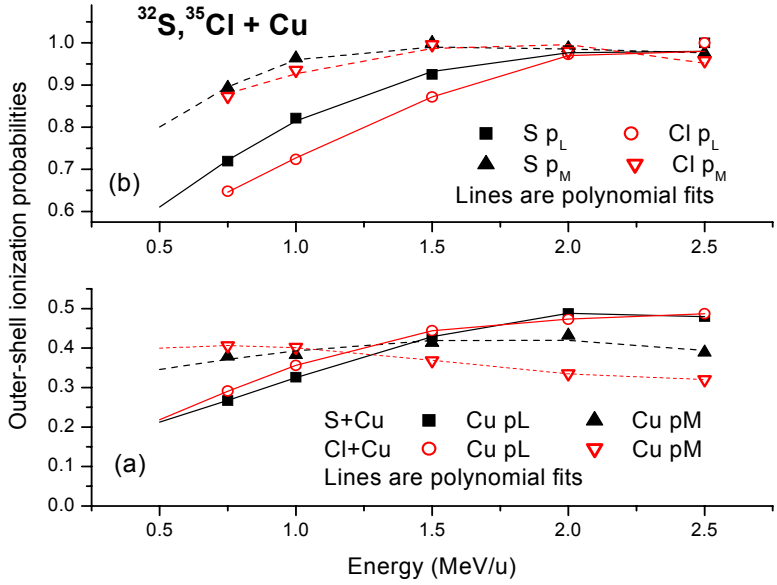

Fig. 8 – Experimental target (a) and projectile (b) L- and M-shell ionization probabilities per electron in the collisions ^{32}S+Cu (full symbols) and ^{35}Cl + Cu (open symbols), in dependence of collision energy. The lines are fits to data.

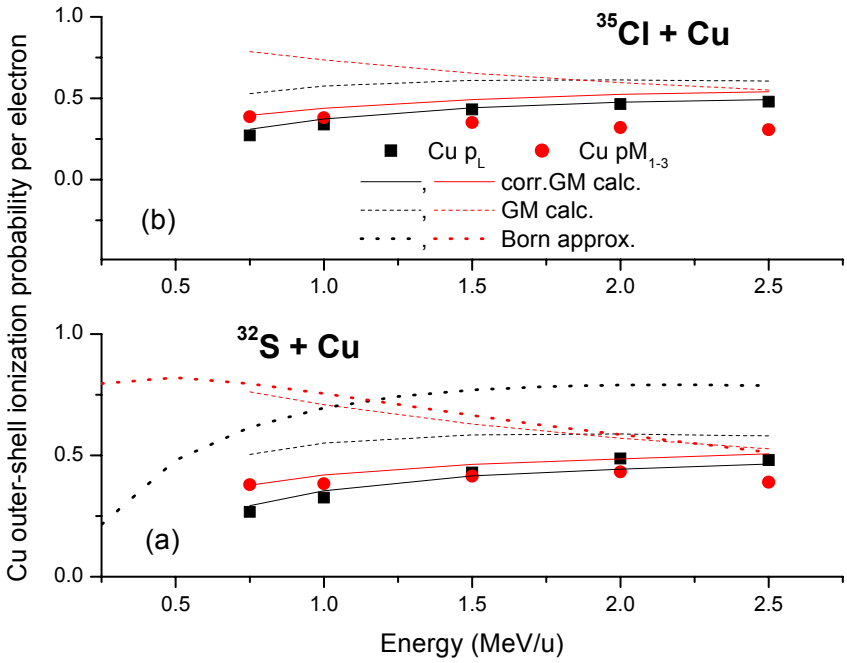

Fig. 9 – Target atom (Cu) outer-shell ionization probabilities per electron, noted p_L and p_{M1-3} for L- and M_{1-3} -shells, respectively, in comparison with model prediction, in the collisions ^{32}S + Cu (a) and ^{35}Cl + Cu (b), in dependence of collision energy. The symbols (black and red symbols for L and M_{1-3}, respectively) are explained in the figures. The lines (black and red for L and M_{1-3} shells, respectively) are model predictions: Born approximation (for ^{32}S+Cu collision) and geometrical model (GM) calculations.

Very high p_L and p_M values (> 0.6) have been obtained for projectiles, some around of 1, as seen in Figs. 8b and 10. In Fig. 10 some other data from literature [23, 24] were also included. While the S p_M values of ref. [23] are in agreement with the present data, the cited from literature S and Cl p_L values are lower.

Worth to mention that, in the present cases of strong multiple ionization, especially, in the case of projectile outer-shells, we are in a limit situation for the applicability of both the experimental determination of p_L and p_M by the yield and energy shifts method and the GM model calculations.

As seen in the Figs. 9 and 10, except the present Cu p_L, where predictions of corr. GM are rather close to data, in all the other cases there is a large discrepancy between predictions and experimental data. In the case of Cu p_M and all projectile outer-shell multiple ionization probabilities (Fig. 10), even the energy dependence is different. This comparison suggests that, at least in the cases of strong outer-shell multiple ionization, the binding energy effect could be one of the factors

responsible for the large discrepancy between the multiple ionization data and model predictions.

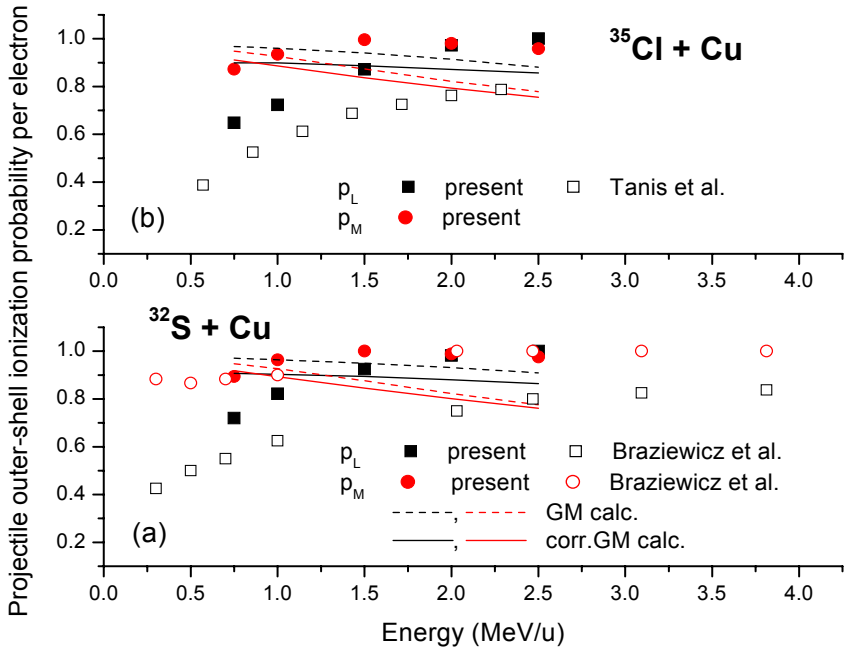

Fig. 10 – The projectile L- and M_{1-3}-shell ionization probabilities per electron for the collisions (a) ^{32}S+ Cu and (b) ^{35}Cl+Cu (full symbols), in dependence of collision energy. The p_L, p_M data for S on Fe targets (Braziewicz et al., [23]) as well as p_L data for Cl on thin C targets (Tanis *et al.*, [24]) (open symbols) are also included. The symbols (black and red symbols for L and M_{1-3}, respectively) are explained in the figures. The lines are the geometric model predictions.

Instead, in the present extreme conditions of strong multiple ionization of the projectile, where the applicability of the above multiple ionization analysis is questionable, we may obtain projectile multiple ionization information independently by the target thickness dependence analysis, as shown in the next section.

The enhancements of K-shell fluorescence yields ω_K obtained from the above multiple ionization analysis, are given in Fig. 11, where two calculation formula (Piticu [13] and Greenberg [21]) were applied. The limit of applicability is appearing in Fig. 11, where the Greenberg's formula applied to projectiles ω_K is leading to very high values, that exceed 1 (the maximum enhancement factors, when ω_K becomes 1, are 12.8 for S and 10.3 for Cl).

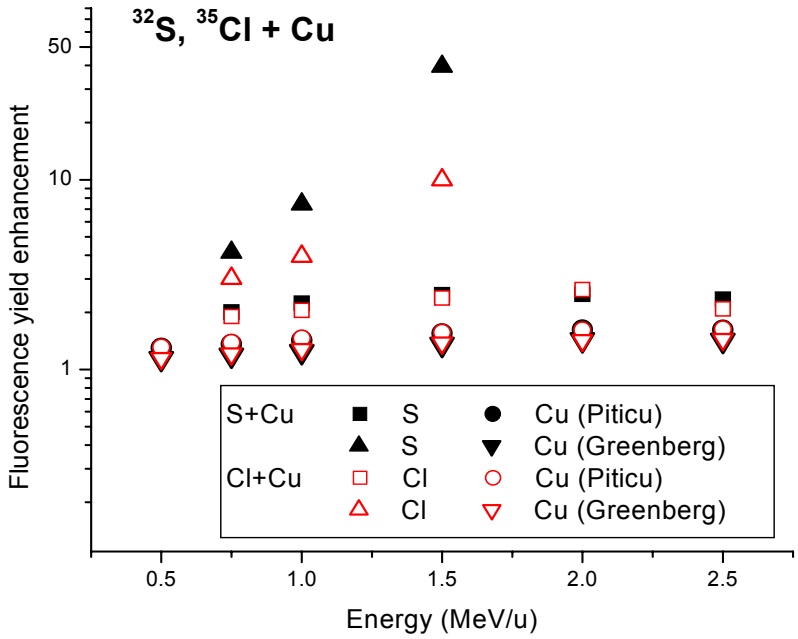

Fig. 11 – Enhancements of the target and projectile K-shell fluorescence yield (ω_K) in the collisions ^{32}S + Cu (full symbols) and ^{35}Cl + Cu (open symbols), in dependence of collision energy. The symbols are explained in the figure. The results of two different procedures for estimating the multiple ionization corrected ω_K (Piticu [13] and Greenberg [21]) are included.

4.2. TARGET THICKNESS DEPENDENCE ANALYSIS

As mentioned before, the target thickness dependence analysis gives information about the outer-shell multiple ionization of the projectile, independently of the analysis in the previous section. In the following figures, the K-shell fluorescence yields ω_K (Fig. 12) and one-vacancy lifetime τ_K (Fig. 13) obtained by target thickness dependence analysis, as enhancement factors relative to tabulated ω_K [20] or theoretical τ_K [25] values, are given. As seen in figures, large enhancements for the projectile K-shell fluorescence yields, by factors up to 11 for S and 6 for Cl, as well as for K-shell vacancy lifetimes, up to 14 for S and 20 for Cl, have been obtained. For comparison, the present estimations using outer-shell multiple ionization analysis (represented as lines in the figures) and some other experimental values from the literature are also included. The two different procedures applied here do not give compatible results, as expected due to the limit conditions for applicability of the multiple ionization analysis. We also mention that the present values for the Cl+ Cu collisions are in good agreement with those obtained by Tanis *et al.* [8] using also target thickness dependence analysis.

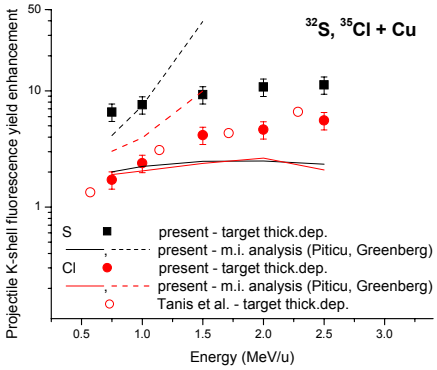

Fig. 12 – Enhancements of the projectile K-shell fluorescence yield (ω_K) in the ^{32}S, ^{35}Cl + Cu collisions (full symbols), determined from the target thickness dependence analysis, in dependence of collision energy. Results of Tanis *et al.* [8] for the Cl+ Cu collision (open symbols) are also included. The symbols are explained in the figure. For comparison, the lines give the present results estimated by multiple ionization analysis.

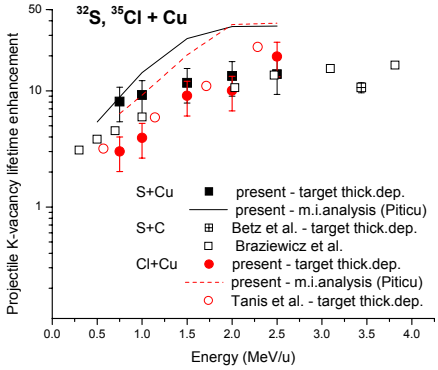

Fig. 13 – Lifetime (τ_K) enhancements of one K-shell vacancy state in the projectile in the ^{32}S, ^{35}Cl + Cu collisions (full symbols), determined from the target thickness dependence analysis, in dependence of collision energy. Other results (Betz *et al.* [4] and Braziewicz *et al.* [23] for S+C and Tanis *et al.* [24] for Cl+ Cu collisions – open symbols) are also included. The symbols are explained in the figure. For comparison, the lines give the present results estimated by multiple ionization analysis.

The fractions of one K-shell vacancy $F_1(\infty)$ used in the target thickness dependence analysis is represented in Fig. 14. For the collision Cl+ Cu, the present values are in agreement with those of ref. [8].

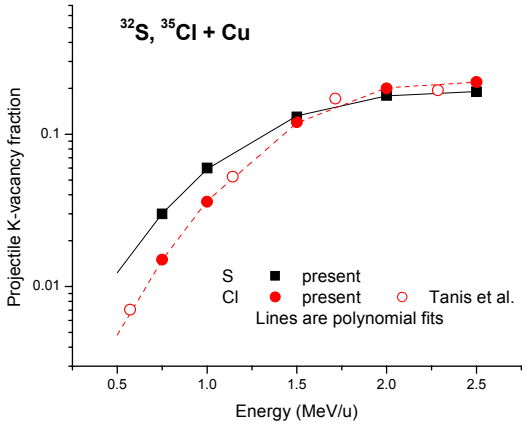

Fig. 14 – Projectile fractions having one K-shell vacancy in the collisions ^{32}S, ^{35}Cl + Cu (full symbols) in dependence of collision energy. The results of Tanis *et al.* [8] for the Cl+ Cu collision (open symbols) are also included. The lines are fits to data.

The K-shell X-ray of the target (Cu) and REC yields obtained in the present experiment are given in Figs. 15 and 16, for ^{32}S+Cu and ^{35}Cl+Cu, respectively, and compared with some theoretical predictions. For comparison, in the case of Cl+ Cu collision, the results of ref. [8], which are in good agreement with the present results, are also included

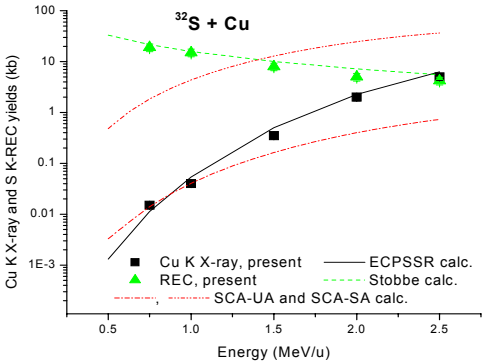

Fig. 15 – Target (Cu) K X-ray and K-REC yields in the ^{32}S + Cu collision in dependence of collision energy. The lines give model predictions (see text).

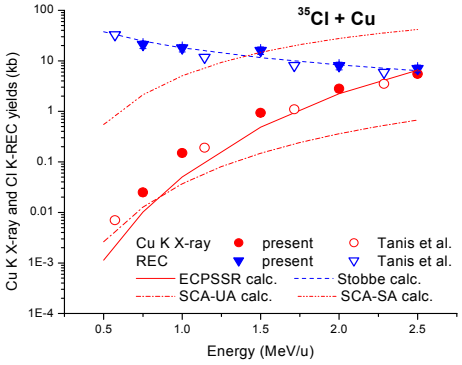

Fig. 16 – The same as Fig. 16 for the case of ^{35}Cl + Cu collision. Present data (full symbols) and data of Tanis *et al.* [8] (open symbols) are included.

For the Cu K X-ray production, the results of SCA calculations [26] in two limit cases, united atom (UA) and separated atom (SA), as well as the ECPSSR predictions [27, 28] have been represented. The present target (Cu) K X-ray production cross sections are placed as expected between the two limit cases of SCA; they are instead in fair agreement with ECPSSR model predictions, for both collisions. The REC theoretical predictions (Stobbe calculations [29], giving the capture cross section per electron, times 11 – the number of "loosely" bound electrons in the Cu atom) are in good agreement with the present data, for both collision systems.

In Fig. 17, the results obtained for the projectile K-shell ionization cross sections are given. Data of ref. [8] which are in fair agreement with the present ones are also included. For comparison, calculations of the ECPSSR model for the inverse collisions (where Cu is the projectile) have been also represented as lines in the figure. As expected, they are not in agreement with the data.

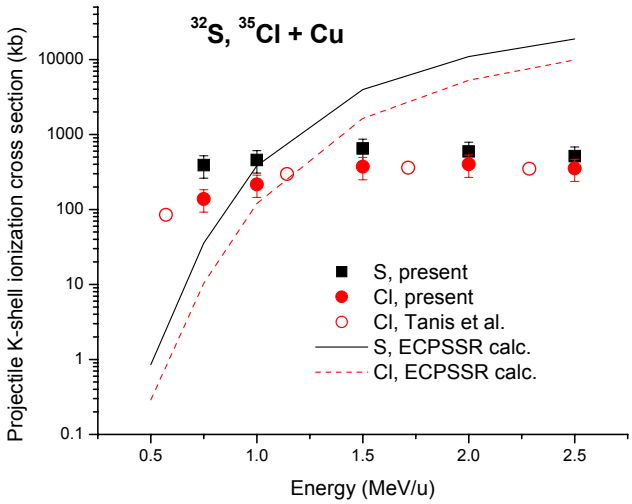

Fig. 17 – Projectile (S and Cl) K-shell ionization cross sections in the ^{32}S, ^{35}Cl + Cu collisions in dependence of collision energy. Present data (full symbols) and data of Tanis *et al.* [8] for the Cl+ Cu collision (open symbols) are included. For comparison, the lines give the ECPSSR predictions for the inverse collisions.

5. SUMMARY AND CONCLUSIONS

In summary, from the measured target thickness dependences of K X-ray and REC yields for 0.75 – 2.5 MeV/u ^{32}S, ^{35}Cl + Cu collisions, the K X-ray production for both partners and REC cross sections, in dependence of collision energy, have been determined.

The present data for Cl+ Cu collision are generally in agreement (within the error bars) with the data reported by Tanis *et al.* [8]. The present target (Cu) K X-ray production cross sections are in fair agreement with ECPSSR model [27, 28] predictions, for both collision systems. Also, the REC theoretical predictions (Stobbe [29] calculations times 11, the number of "loosely" bound electrons in Cu) are in fair agreement with the present data, for both collision systems.

By analysis of outer-shell multiple ionization with the procedure of "yield and energy shifts" [13], the outer-shell multiple ionization probabilities per electron p_L and p_M have been estimated. Generally, the calculations of the geometrical model (GM) [22] are not in agreement with the present data. Except the present Cu p_L, where predictions of corr. GM (GM with corrected binding energies) are rather close to data, in all the other cases there is a large discrepancy between predictions and experimental data. We suggest that at least in the case of strong outer-shell multiple ionization, the binding energy effect could be a plausible reason for this situation.

Large enhancements of the projectile K-shell fluorescence yields, attaining values as high as 0.5 in Cl and 0.9 in S, have been obtained. Also, increased K-shell vacancy lifetimes, by factors up to 14 for S and 20 for Cl, have been estimated.

REFERENCES

1. H. D. BETZ and L. GRODZINS, Phys. Rev. Lett., **25**, 211 (1970).
2. H. BRÄUNING *et al.*, Physica Scripta T, **92**, 43 (2001).
3. I.Y. TOLSTIKINA and V.P. SHEVELKO, AIP Conf. Proc., **740,** 59 (2004).
4. H.-D. BETZ *et al.*, Phys. Rev. Lett., **33**, 807 (1974).
5. F. HOPKINS, Phys. Rev. Lett., **35**, 270 (1975).
6. T.J. GRAY *et al.*, Phys. Rev. A, **14,** 1333 (1976).
7. R.K. GARDNER *et al.*, Phys. Rev. A, **15**, 2202 (1977).
8. J.A. TANIS *et al.*, Phys. Rev. A, **22**, 483 (1980).
9. J. HALL *et al.*, Phys. Rev. A, **28**, 99 (1983); A **33**, 914 (1986).
10. L.C. TRIBEDI *et al.*, Z. Phys. D, **24**, 215 (1992); D **27**, 143 (1993).
11. B.B. DHAL *et al.*, Phys. Rev. A, **62**, 022714 (2000).
12. A.C. SCAFEŞ *et al.*, Phys. Scripta, 2013 accepted for publication.
13. A. BERINDE *et al.*, *Atomic and Nuclear Heavy Ion Interactions*, Proc. Int. School on Physics, Brasov, Romania, 1984, Eds. A. Berinde et al. (CIP, Bucharest, 1986), Vol. **1**, p. 453 and 461.
14. A.C. SCAFEŞ *et al.*, Rom. Rep. Phys., **66**, 455 (2013).
15. I.P. GRANT *et al.*, Computer Physics Communications, **21**, 207 (1980).
16. E. STORM and H.I. ISRAEL, Nucl. Data Tabl. A, **7**, 565 (1970).
17. R. SHULE *et al.*, J. Phys. B, **10,** 889 (1977).
18. K. TAULBJERG *et al.*, Phys. Rev. A, **12,** 2325 (1975).
19. W.E. MEYERHOF, Phys. Rev. Lett., **31,** 1341 (1973).
20. M.O. KRAUSE, J. Phys. Chem. Ref. Data, **8**, 307 (1979).
21. J.S. GREENBERG *et al.*, Phys. Rev. A, **16,** 964 (1977).
22. B. SULIK *et al.*, J. Phys. B, **17,** 3239 (1984); Nucl. Instrum. Methods B **28,** 509 (1987).
23. J. BRAZIEWICZ *et al.*, Phys. Rev. A, **82**, 022709 (2010).
24. J.A. TANIS *et al.*, Phys. Rev. A, **27,** 1671 (1983).
25. E.J. McGUIRE, Phys. Rev. A, **2**, 273 (1970).
26. D. TRAUTMANN and F. RÖSEL, Nucl. Instrum. Methods, **169**, 259 (1980).
27. W. BRANDT and G. LAPICKI, Phys. Rev. A, 23 (1981) 1717.
28. V. HORVAT, Computer Physics Communications, **180** (2009) 995.
29. M. STOBBE, Ann. Phys., **7** (1930) 661.